Proceedings of Meetings on Acoustics

Volume 20, 2013 http://acousticalsociety.org/

## 166th Meeting of the Acoustical Society of America
## San Francisco, California
## 2 - 6 December 2013

## Session 3pPAa: Physical Acoustics

# 3pPAa1. Sensitivity analysis of an equivalent source model for military jet aircraft noise

**Tracianne B. Neilsen*, Kent L. Gee, David M. Hart and Michael M. James**

***Corresponding author's address: Dept. of Physics and Astronomy, Brigham Young University, N311 ESC, Provo, Utah 84602, tbn@byu.edu**

The noise from a tied-down F-22A Raptor is modeled with an equivalent source consisting of two line arrays of monopole sources and their image sources, to represent the interference from the ground. These arrays, one correlated and one uncorrelated, with Rayleigh-distributed amplitudes, mimic properties of fine and large-scale turbulent mixing noise. [Morgan et al., Noise Control Eng. J. 60, 435-449 (2012)]. The equivalent source modeling parameters (the distributions' peak locations, amplitudes, widths, and the relative phase angle between correlated sources) are selected using Bayesian optimization implemented with simulated annealing and fast Gibbs sampler algorithms. The resulting equivalent source model reasonably predicts the radiated midfield up to 1250 Hz [Hart et al., POMA 19, 055094 (2013)]. In this study, the relationship between the correlated array's peak location and its phase angle has been further analyzed. Although sensitivity analysis of the results reveals non-uniqueness of the model, it also yields additional physical insight in the form of bounds for the dominant aeroacoustic source region as a function of frequency. The far field sound radiation predicted by the equivalent source model for a wide range of frequencies will be compared to measured far-field directivities. [Sponsored by the Office of Naval Research.]

Published by the Acoustical Society of America through the American Institute of Physics

 [DOI: 10.1121/1.4865249]
Received 22 Jan 2014; published 29 Jan 2014

## INTRODUCTION

An equivalent source model (ESM) collapses the complex, turbulent flow into a set of wave functions or source parameters that describe the salient features of the radiated acoustic field. It is a non-unique description that results from an optimization process and therefore describes the field in a least-mean squares sense. The alteration of the source description with frequency and flow conditions yields an efficient means of correlating the acoustic and flow parameters. The ESM formulation, i.e. the choice of wave functions or sources, depends on the nature of the problem. Lighthill's quadrupole description of free jet noise[1] was essentially an ESM. Various types of ESM have been applied to aeroacoustics related problems, including the calculation of combustion noise[2] and noise radiated from a high-bypass jet engine nacelle.[3]

Two ESMs that have been employed for jet noise mention merit here. The first is a description of the source in terms of wavepackets. These wavepackets consist of traveling waves with finite extent whose amplitudes grow and decay as a result of turbulence instabilities; they are responsible for correlated noise generation through Mach wave radiation. Source characterization and radiation based on wave packet models have been described by Suzuki and Colonius,[4] Reba *et al*.,[5] etc. The different spectral shapes seen in supersonic jet noise to the sideline (rounded) and downstream (peaked) have been described in terms of wavepacket broadening by Papamoschou.[6] Results of near-field acoustical holography on a military jet have been connected to wavepackets in a recent paper by Wall *et al*.[7]

A second approach builds off the work by Tam *et al*., [8-11] who have described supersonic jet noise radiation in terms of two types of spectra – the rounded and peaked spectra that exist in different directions, and combinations of the two at intermediate angles. This two-source model served as the foundation for an ESM we are developing for military jet aircraft noise radiation. The source is represented by line arrays of correlated and uncorrelated monopoles and, to account for the hard ground, their images. The amplitude variation for both types of sources is assumed to follow Rayleigh distributions whose peak locations, widths, and amplitudes, along with the phase angle for the correlated sources, are adjusted to minimize the mean-square error along a portion of the measurement surface. Once the monopole source strengths have been found as a function of frequency, they can be used to predict the levels elsewhere. Initial applications of this ESM are found in Refs. [12] and [13]. However, the resulting data-based parameter estimates are inherently nonunique. Consequently, there is a strong correlation between subsets of these parameters such that a range of combinations exist that produce similar answers and add uncertainty to the model.

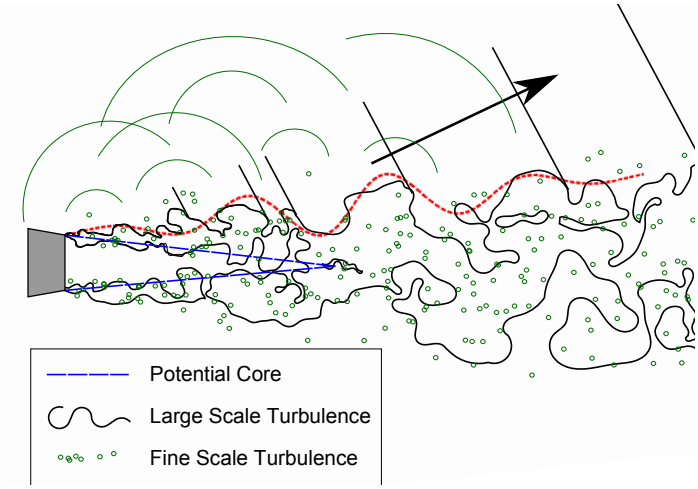


**Figure 1 Illustration of the two types of turbulent mixing noise in a jet.**

The mathematical formulation of this simple-source ESM is found in more depth in Ref. [12], but a summary is provided here. For the uncorrelated line array and its image, the total squared pressure at frequency $f$ and location $\vec{r}$ is calculated by adding up the contribution of the monopoles, with amplitudes $A_m$, incoherently:

$$P_{T,u}^2 = \sum_{m=1}^{N}[A_{m,u}[G(\vec{r},\vec{r}_{D_m}) + \tilde{Q}_m G(\vec{r},\vec{r}_{I_m})]]^2, \quad (2)$$

where $\tilde{Q}_m$ denotes the spherical reflection coefficient (set equal to one to model the concrete run-up pad), and subscript $u$ indicates that this is the uncorrelated contribution to the field. In the case of correlated sources, the total squared pressure is the coherent sum over the individual monopoles:

$$P_{T,c}^2 = [\sum_{m=1}^{N} \tilde{A}_{m,c}[G(\vec{r},\vec{r}_{D_m}) + \tilde{Q}_m G(\vec{r},\vec{r}_{I_m})]]^2. \quad (3)$$

The correlated amplitude distribution is

$$\tilde{A}_{m,c}(z_m, \Delta z, \sigma) = A_m(z_m, \Delta z, \sigma)e^{j\varphi m}, \quad (4)$$

where $\varphi$, the phase difference from one monopole to the next, is [14]

$$\varphi = \frac{2\pi f d\cos\theta}{c}. \quad (5)$$

The space between the monopoles, $d$, is small enough to simulate a continuous source, $c$ represents sound speed, and $\theta$ is the directivity angle. The correlated and uncorrelated line arrays are combined to give the total squared pressure:

$$P_T^2 = P_{T,c}^2 + P_{T,u}^2. \quad (6)$$

At each frequency of interest, this total, modeled, squared pressure is propagated via the Green's function to multiple observation points, which correspond to the microphone locations, and yields a planar map of the sound field to compare with the measured data.

As with previous related papers,[12,13] a Rayleigh distribution is used to compute the relative amplitudes of the monopoles as

$$\left|\tilde{A}_m(z_m, \Delta z, \sigma)\right| = A_{\max}\frac{z_m - \Delta z}{\sigma^2}e^{\frac{-(z_m-\Delta z)^2}{2\sigma^2}} = A_m(z_m, \Delta z, \sigma), \quad (1)$$

where $z_m$ is the location of the $m^{\text{th}}$ monopole, $A_{\max}$ is the peak amplitude in the distribution, $\Delta z$ is distance the peak of the distribution has been shifted downstream, and $\sigma$ is the relative width of the distribution. (See Figure 2.)

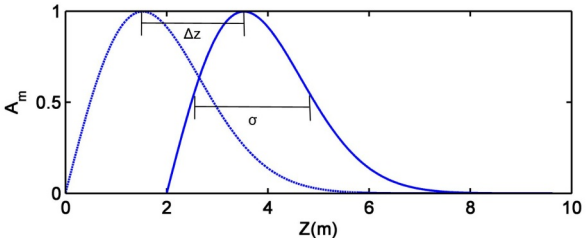


**Figure 2. A Rayleigh distribution (dotted line), which rises quickly and decays slowly, and a shifted distribution (solid line), labeled with the shift distance, Δz, and the scale parameter, σ.**

The parameters that control the maximum amplitude, the width, and the location of the peak for the correlated (subscript $c$) and the uncorrelated (subscript $u$) distributions are varied in the ESM. Specifically, the peak locations $\{z_{p,u}, z_{p,c}\}$, widths $\{\sigma_u, \sigma_c\}$, and the ratio of the maximum amplitudes of the two arrays $\{A_{m,c}/A_{m,u}\}$, and the source phase angle, $\theta$ are variables. The model's parameters are adjusted to create a source that gives the least square error between the model and measured data.

The initial implementation of this simple-source ESM used the sound field measured on large planes in the vicinity of a tied-down F-22A Raptor. One engine was operated at idle, intermediate, military and afterburner engine

conditions, while the other engine was held at idle. All results shown in this paper are for measurements at afterburner for some of the locations illustrated in Figure 3. A complete description of the experiment is found in Wall et al.[15] Examples of the noise content for different frequencies across the 2 m high by 23 m long planes are shown in subsequent figures. Above about 200 Hz, one or more strong interference nulls runs through the planes.

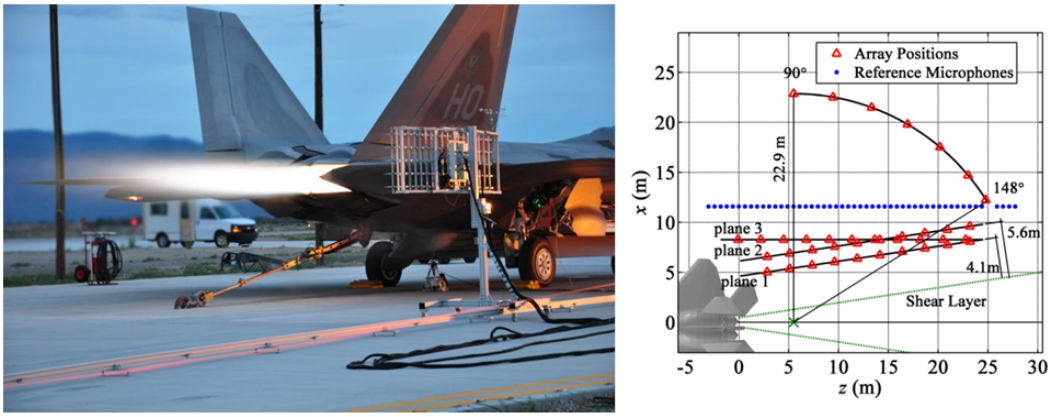


**Figure 3. (left) A picture of the F22-A Raptor with the microphone array. (right) Schematic of the measurement locations relative to the jet. The red triangles indicate the locations at which the microphone array was positioned during the experiment. The estimated shear layer is marked by green dashed lines, and the green "x" delineates the estimated maximum-noise-source region and arc origin.**

In Morgan *et al.*,[12] the ESM was formulated by manually adjusting the parameters and using fixed source phase angle derived from far-field directivity measurements. In Hart *et al.*,[13] a Bayesian optimization algorithm was used to obtain maximum likely values and estimated posterior probability distributions. In both cases, the data-based source strengths were similar to what was expected from the previous beamforming results of Lee and Bridges:[16] the maximum source region contracts and moves upstream as the frequency increases. In both cases, similar results gave insight into the nature of the relationship between the ESM parameters and the measured field:

(1) Interference nulls are much deeper for model than measurements because the model does not include the volumetric nature of the source. To compensate for this, only locations at which the measured SPL is within 40 dB of the maximum are used to calculate the mismatch between modeled field and measurements.

(2) The correlated portion of the ESM controls the primary features of the match between modeled and measured levels at frequencies below 500 Hz. A Rayleigh distribution of the source amplitude for these correlated sources can reproduce the location and orientation of the interference nulls.

(3) The agreement between model and measurement is less sensitive to changes in uncorrelated source parameters. However, in some cases, minor adjustments in the uncorrelated source parameters can improve match to the side of nozzle at higher frequencies. It is likely that the Rayleigh distribution is not the best choice for the uncorrelated portion of the ESM.

This paper presents a study of the relationship between the correlated source parameters of the simple-source ESM. A least-squares cost function quantifies the mismatch between the measured and predicted fields across the large planes of data shown in Figure 2. In particular, the interdependence of the location of the source distribution peak for the correlated portion of the ESM and the directivity angle that controls the phase relationship between the monopoles is investigated.

## RESULTS

Parameter selection for the ESM relies upon quantifying the agreement between measured levels and predicted levels. While the parameter selection can be done manually, an automated algorithm for estimating the parameters provides a more objective answer, which is necessary for obtaining a reasonable model when the answer is not known. The resulting modeling parameters are inherently uncertain. In many cases, some modeling parameters have minimal effect on the measurement/model agreement. The estimates obtained for these parameters likely have

little physical significance. On the other hand, the key modeling parameters are the ones that primarily determine whether the ESM yields a suitable prediction of the measured field.

Previous studies of the simple-source ESM by Hart *et al.*[13] showed that the parameters related to the correlated source primarily determine how well the ESM predicts the measured field. These primary parameters are the peak location and the scale parameter of the Rayleigh distribution for the correlated line arrays, $z_{p,c}$ and $\sigma_c$, (see Figure 2) and the source phase angle, $\theta$. However, the estimates obtained for these parameters are not independent. There is a correlation between values of these parameters that result in approximately the same agreement between the model and the data. An example of this can be seen in Figure 4, which provides snapshots of the three-dimensional search space of these primary parameters. The color bar indicates the value of the least-squares cost function when 630 measurement locations on planes 1 and 2 in Figure 3 were included in the calculation. The dark regions indicating good agreement between the field predicted by the ESM and the measured one illustrate the valley in the search space. The presence of this valley means that there is a natural correlation between these parameters, such that model/data mismatch defined by the least-squares cost function cannot distinguish meaningfully between combinations that lie in the valley. This provides an idea of the uncertainty in the parameter estimates.

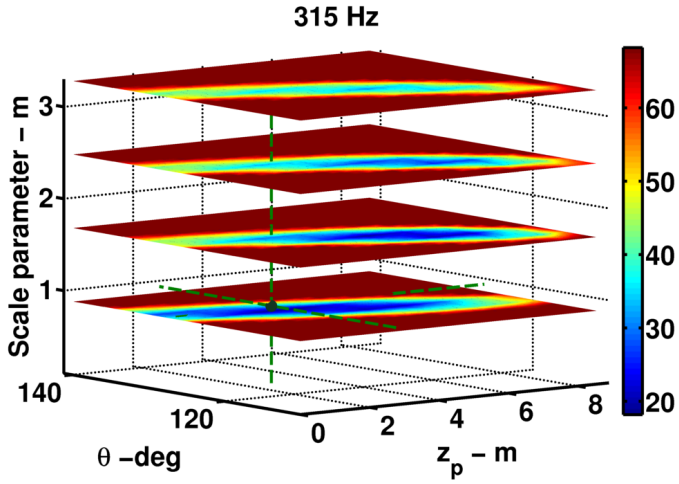


**Figure 4. Maps of the value of the least-squares cost function in the ESM parameter search space, at 315 Hz using the data from planes 1 and 2, as a function of source phase angle $\theta$, peak location $z_{p,c}$of the Rayleigh distribution describing the amplitude of the monopoles on the correlated line array (and its image) for four values of the scale parameter, $\sigma_c$, of the Rayleigh distribution. The other three parameters were held at nominally ideal values. The black dot and accompanying green dashed lines show the solution obtained by the optimization for this case.**

To investigate the natural correlations between the source phase angle, $\theta$, and peak location of the Rayleigh distribution, $z_{p,c}$, a Levenberg-Marquardt algorithm (LMA) was applied to minimize the least-squares cost function. Unlike the Bayesian optimization algorithms (BOA) applied by Hart et al,[13] the LMA uses gradient information to estimate the step sizes in the parameters that will likely move the solution towards the minimum. In addition, the parameters were not forced to stay within bounds, as in the BOA, but a penalty was added if the selected parameter was outside the specified limits. This was an important consideration because at lower frequencies (below 500 Hz) the derivatives associated with the parameters defining the uncorrelated line array's amplitude distribution are extremely small, such that the LMA often selects values for these parameters outside the realistic source region. As the frequency increases (where the uncorrelated sources contribute more to the field), the corresponding derivatives increase, and the sampled values for these uncorrelated parameters stay within the physical bounds.

Estimates of $\theta$ and $z_{p,c}$ from several LMA optimizations, based on the data from plane 1 and different initial parameter values, are summarized in Figure 5. For each frequency the combinations of $\theta$ and $z_{p,c}$ at which the optimization ended lie along a different diagonal line. These combinations give comparable least-squares fits, and the spread of the circles gives an idea of the uncertainty associated with the parameter estimates obtained by the optimizations. The "best fit" solution at each frequency is shown by a filled circle and is used in the subsequent discussion of the result.

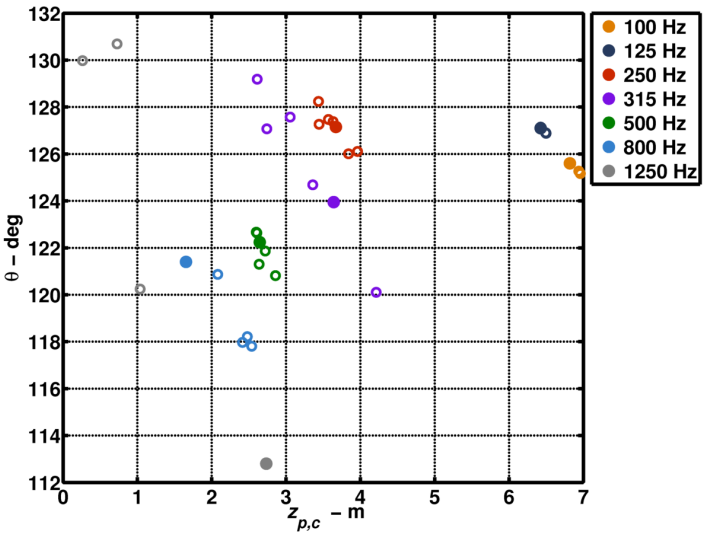


**Figure 5. Estimates of $\theta$ and $z_{p,c}$ obtained by LMA optimizations using the data on plane 1 at different frequencies (represented by color). The filled circles represent the "best fit" solution at each frequency, which is used for the subsequent plots.**

The source distributions for the ESM obtained from the optimizations on plane 1 exhibit many of the characteristics expected for heated, supersonic jet noise, as shown in Figure 6. For frequencies of 315 Hz and below, the correlated source is responsible for the predicted field over the aperture of interest. The location of the peak in the amplitude distribution shifts upstream (close to the jet nozzle) and narrows as the frequency increases. This general trend is expected from previous beamforming results on heated jets.[8,16] At 500 Hz, the amplitude distribution of the correlated source is quite narrow and the uncorrelated source begins to contribute to the predicted field. At 800 and 1250 Hz, the uncorrelated sources are responsible for a large portion of the field. The two-source theory for jet noise supports this increase in the relative importance of the uncorrelated noise as frequency increases.[10,17] (Note that the absolute amplitude values are unimportant as the modeled levels are shifted in the end such that the maximum matches the maximum measured level.)

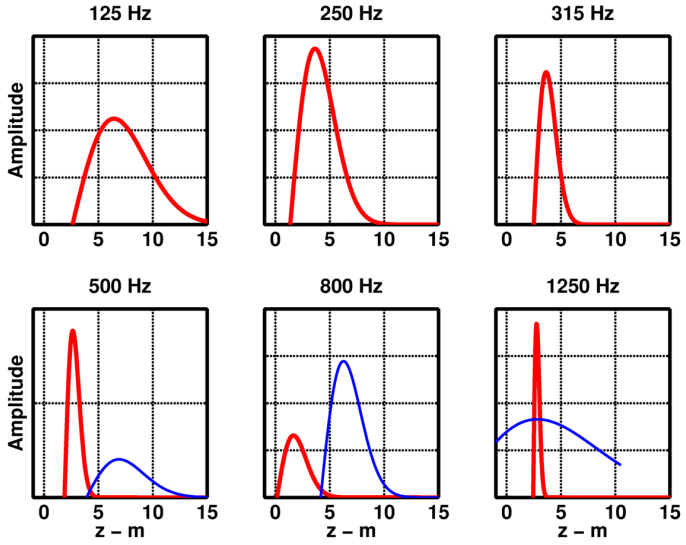


**Figure 6. Source amplitude distributions for the ESM obtained from the LMA optimizations at the frequencies indicated using data from plane 1 (in Figure 3). The red (thicker) lines are for the correlated sources, and the blue (thinner) lines for the uncorrelated sources.**

Maps of the levels computed with the source distributions in Figure 6 are presented in Figure 7 - Figure 12 and illustrate the capabilities and limitations of the simple-source ESM. For each frequency, the top plot contains the levels on plane 1 predicted by the ESM, the middle plot contains the measured levels on plane 1, and the lowest plot shows both the predicted and measured levels across the top of the array when is was located along an arc 22.9 m from the estimated maximum source region. The agreement between the ESM and the data is quite good at 315 Hz and below at both locations. At these frequencies, the line array of correlated monopoles and its image capture the general features of the field. The portions of the field that are not in agreement are in most cases related to what has been termed the "double-peak" in Ref. [18], which would not be captured by the ESM. The double peak refers two two discrete maxima in the spectra at one location and two distinct directivity lobes at frequencies near the peaks. At 500 Hz and above, the ESM predict the locations of the interference nulls but produced longer tails than measured. At 500 and 800 Hz, the ESM also does not represent the wide spread of energy near the jet nozzle. It is likely that the limitations with the ESM at these higher frequencies relates to the lack of the Rayleigh distribution to represent the sources. Likely a different distribution with a more gradual rise and shorter tail would work better at the higher frequencies.

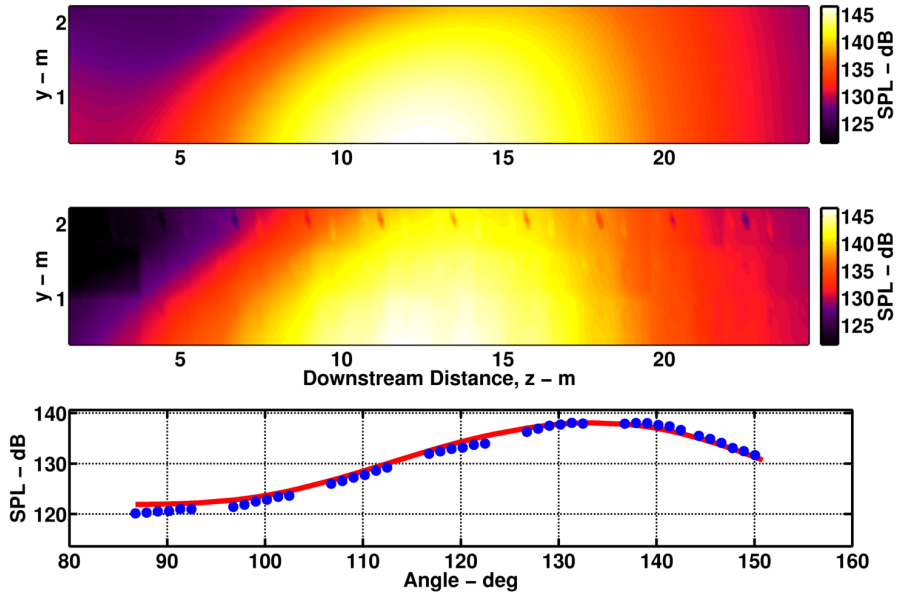


**Figure 7 Comparison of the levels on plane 1 predicted by the ESM (top) and measured (middle) near the F-22A Raptor in 2009 (See Figure 3) at 125 Hz. The modeling parameters obtained using the data on plane 1 were also used to compute the field along an arc at 22.9 m from the estimated maximum source region (bottom). The blue circles display the measured levels and the red line the predicted levels.**

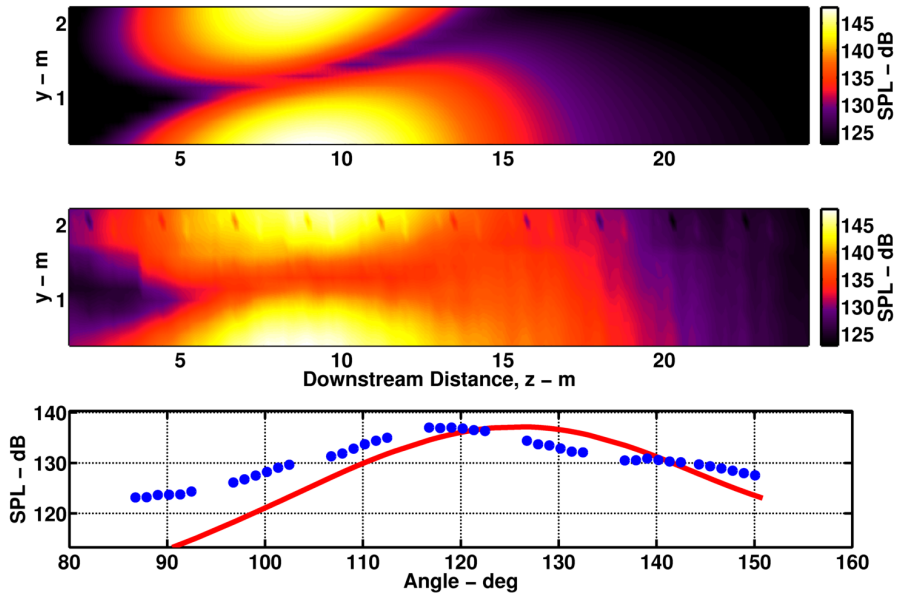


**Figure 8. Same as Figure 7, but at 250 Hz.**

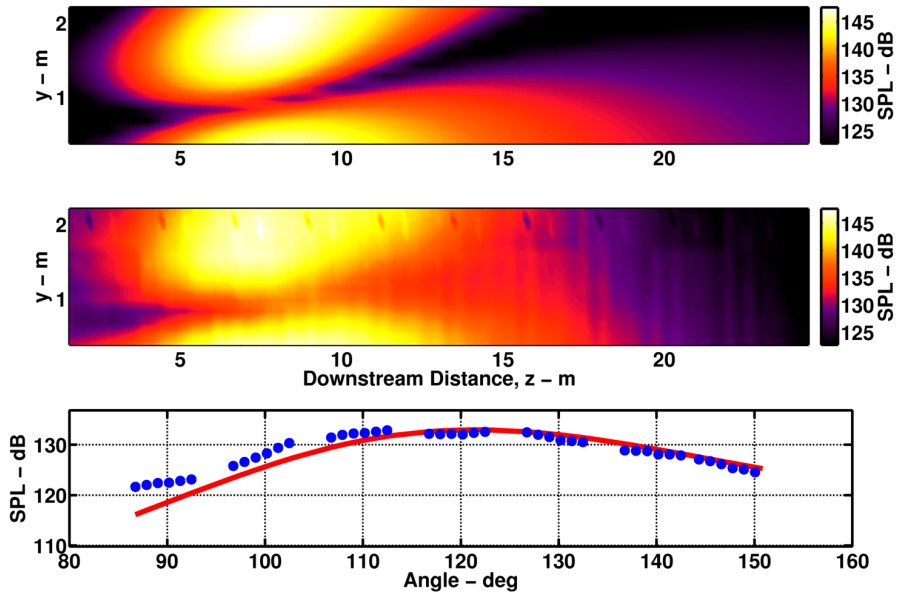


**Figure 9. Same as Figure 7, but at 315 Hz.**

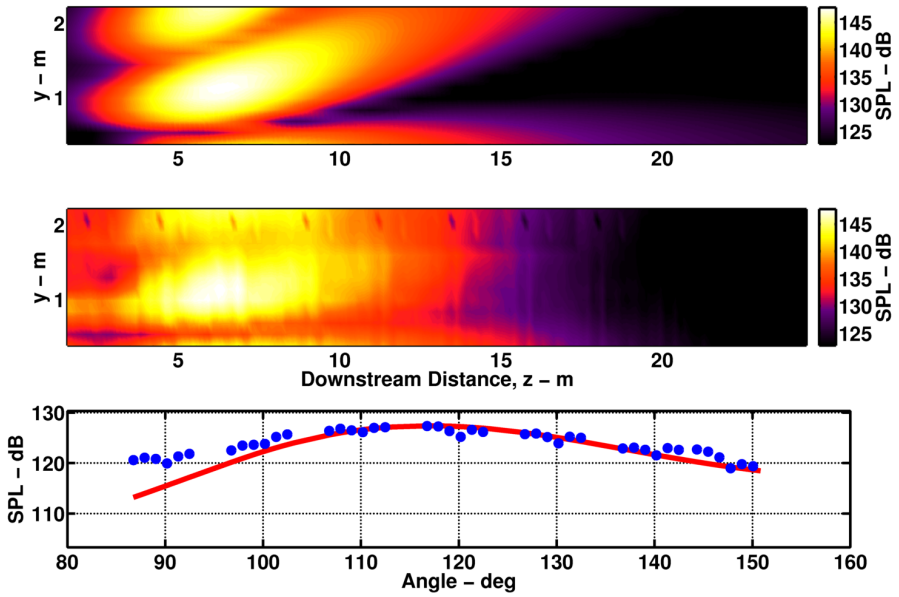


**Figure 10. Same as Figure 7, but at 500 Hz.**

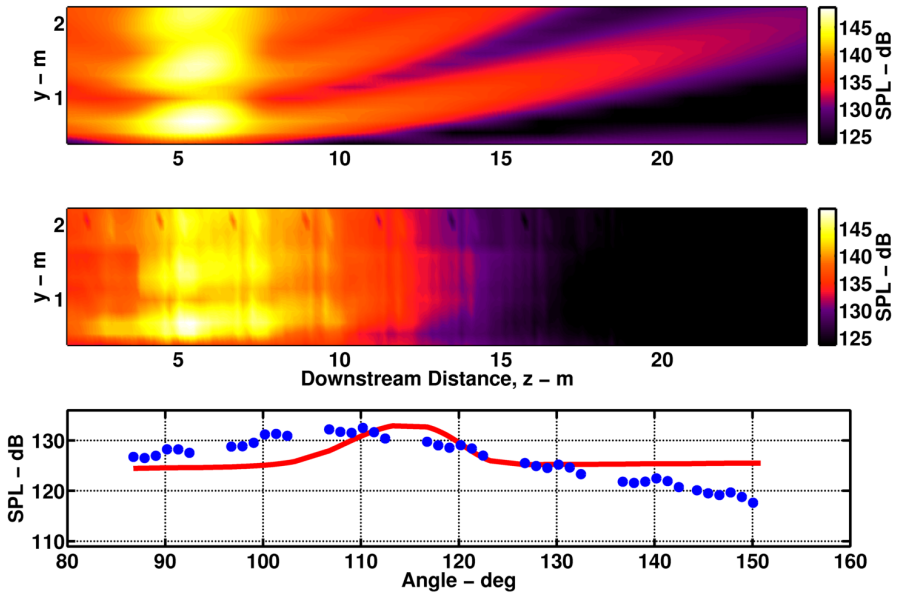


**Figure 11. Same as Figure 7, but at 800 Hz.**

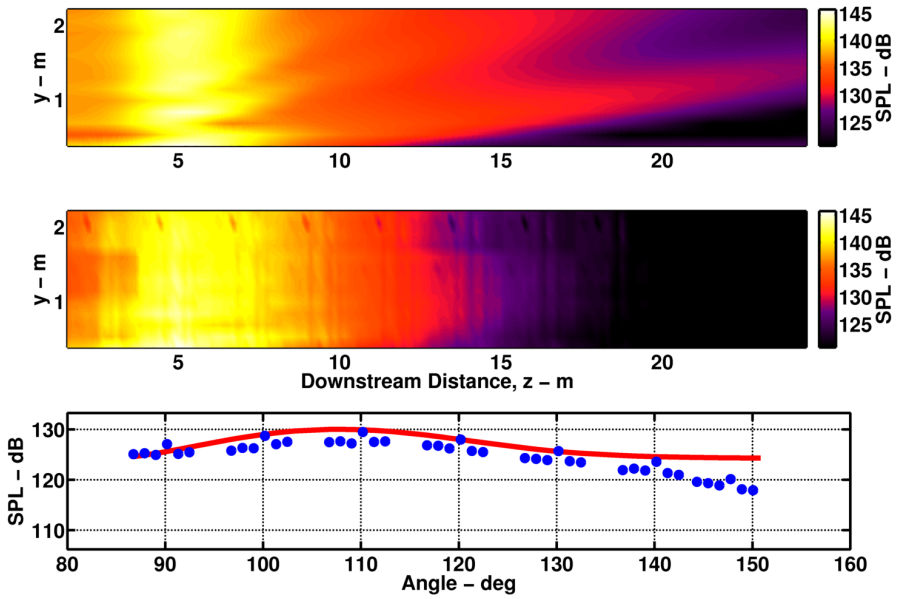


**Figure 12. Same as Figure 7, but at 1250 Hz.**

## CONCLUSION

The simple-source ESM presented in this paper predicts the major features of the sound field in the vicinity of an F-22A Raptor at afterburner. The two line arrays, representing correlated and uncorrelated noise and their images with Rayleigh distributions for the source amplitudes, provide a description of an equivalent source that generates noise similar to the high-temperature, supersonic jet. However, there is an inherent uncertainty in the parameter estimates obtained. First, the uncorrelated source parameters appear to be insignificant at frequencies below 500 Hz. Second, the interdependence of the parameters for the correlated source creates valleys in the parameter search space such that combinations of the phase angle and location of the peak in the distribution give essentially the same agreement. Nevertheless, the reasonable predictions obtained by this simple-source model are intriguing. Future improvements to the ESM may include varying the amplitude distribution shape as a function of frequency to account for the shorter tails at higher frequencies and including volumetric nature of source such that the predicted interference nulls are less pronounced.

Despite the straightforward nature of this ESM, there may be more physical insight to be obtained by comparing with other ESMs based on wavepackets. In the current model, the correlated portion of the ESM is responsible for the dominant noise generation along the direction of maximum overall sound pressure level. (See Ref. [15].) The real part of the complex correlated source distributions, shown in Figure 13, are reminiscent of the wavepackets used in other ESMs.[4-6,19] The relationship between this correlated portion of this simple-source model and the wavepackets, which are both associated with large-scale noise generation, needs to be investigated.

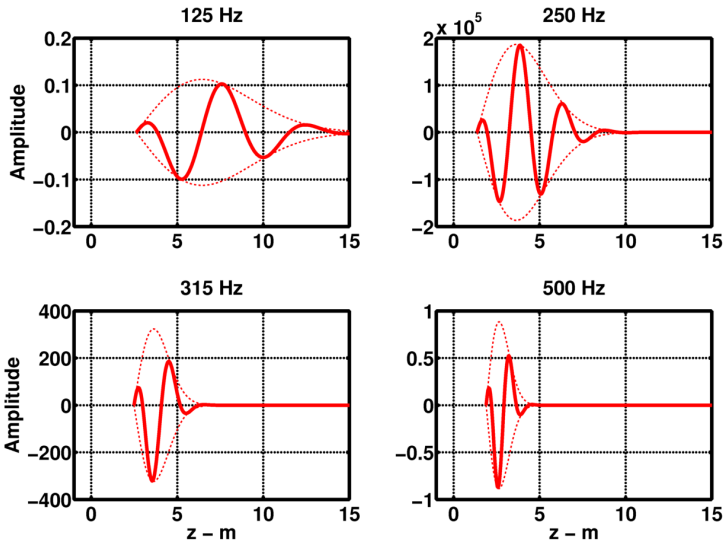


**Figure 13. The real portions (solid) and amplitudes (dotted) of the source distributions for the correlated line array at 125, 250, 315 and 500 Hz, for the "best fit" optimization parameters.**

## ACKNOWLEDGEMENTS

The authors gratefully acknowledge funding for this analysis from the Office of Naval Research. The measurements were funded by the Air Force Research Laboratory through the SBIR program and supported through a Cooperative Research and Development Agreement (CRDA) between Blue Ridge Research and Consulting, Brigham Young University, and the Air Force.[20,21]

## REFERENCES

[1] M. J. Lighthill, "On Sound generated aerodynamically. Part 1. General Theory," Proc. R. Soc. London, **211**, 564-587 (1952).
[2] H. Brick, R. Piscoya, M. Ochmann, and P. Koltzsch, "Modeling of combustion noise with the Boundary Element Method and Equivalent Source Method," Proc. Internoise 2004 (2004).
[3] F. Holste, "An equivalent source method for calculation of the sound radiated from aircraft engines," J. Sound Vib. **203**, 667-695 (1997).
[4] T. Suzuki and T. Colonius, "Instability waves in a subsonic round jet detected using a near-field phased microphone array," J. Fluid Mech. **565**, 197–226 (2006).
[5] R. Reba, S. Narayanan and T. Colonius, "Wave-packet models for large-scale mixing noise," Int. J. of Aeroacoustics **9**, 533-558 (2010).
[6] D. Papamoschou, "Wavepacket modeling of the jet noise source," AIAA Paper 2011-2835 (2011).
[7] A. T. Wall, K. L. Gee, T. B. Neilsen and M. M. James, "Acoustical holography and proper orthogonal decomposition analyses of full-scale jet source properties," J. Acoust. Soc. Am. **134**, 4127 (2013).
[8] C. K.W. Tam, K. Viswanathan, K. K. Ahuja, and J. Panda, "The sources of jet noise: experimental evidence," J. Fluid Mech., **615**, 253-292 (2008).
[9] C. K. W. Tam, M. Golebiowski, J. M. Seiner, "On the Two Components of Turbulent Mixing Noise from Supersonic Jets," AIAA paper 96-1716 (1996).
[10] C. K. W. Tam, N. N. Pasouchenko, and R. H. Schlinker, "Noise source distribution in supersonic jets," J. Sound Vib. **291**, 192-201 (2006).
[11] K. Viswanathan, "Mechanisms of jet noise generation: Classical theories and recent developments," Int. J. of Aeroacoustics **8**, 355-407 (2009).
[12] J. Morgan, T. B. Neilsen, K. L. Gee, A. T. Wall, and M. M. James, "Simple-source model of high-power jet aircraft noise," Noise Control Eng. J. **60**, 435-449 (2012).

[13] D. M. Hart, T. B. Neilsen, K. L. Gee, and M. M. James, "A Bayesian-based equivalent sound source model for a military jet aircraft," Proc. Mtgs. Acoust. **19**, 055094 (2013).
[14] A sine function appears in the original publication of Ref [12]. However, a cosine corrects for an ambiguity in the reference point and assumes $\theta$ is measured from the jet inlet.
[15] A. T. Wall, K. L. Gee, M. M. James, K. A. Bradley, S. A. McInerny, and T. B. Neilsen, "Near-field noise measurements of a high-power jet aircraft," Noise Control Eng. J. **60**, 421-434 (2012).
[16] S. S. Lee and J. Bridges, "Phased-Array Measurements of Single Flow Hot Jets," AIAA Paper 2005–2842 (2005).
[17] T. B. Neilsen, K. L. Gee, A. T. Wall, and M. M. James, "Similarity spectra analysis of high-performance jet aircraft noise," J. Acoust. Soc. Am. **133**, 2116 – 2125 (2013).
[18] T. B. Neilsen, K. L. Gee, and M. M. James, "Spectral characterization in the near and mid-field of military jet aircraft noise, AIAA paper 2013-2191 (2013).
[19]P. Jordan and T. Colonius, "Wave packets and turbulent jet noise," Annu. Rev. Fluid Mech. **45**, 173–95 (2013).
[20] SBIR DATA RIGHTS - (DFARS 252.227-7018 (JUNE 1995)); Contract Number: FA8650-08-C-6843; Contractor Name and Address: Blue Ridge Research and Consulting, LLC, 15 W Walnut St. Suite C; Asheville, NC Expiration of SBIR Data Rights Period: March 17, 2016 (Subject to SBA SBIR Directive of September 24, 2002) *The Government's rights to use, modify, reproduce, release, perform, display, or disclose technical data or computer software marked with this legend are restricted during the period shown as provided in paragraph (b)(4) of the Rights in Noncommercial Technical Data and Computer Software—Small Business Innovation Research (SBIR) Program clause contained in the above identified contract. No restrictions apply after the expiration date shown above. Any reproduction of technical data, computer software, or portions thereof marked with this legend must also reproduce the markings.*
[21] Distribution A – Approved for public release; Distribution is unlimited 88ABW-2011-5646 and 88ABW-2012-6365.